Synthesis, Characterization, and Study of the Photocatalytic Activity upon Polymeric-Surface Modification of ZnO Nanoparticles

Ahmed Mir

Research Laboratory of Engineering Process and Industrial Systems, National School of Engineers of Gabes, University of Gabes, Tunisia
ahmedmirch@gmail.com (corresponding author)

Nidhal Becheikh

Research Laboratory of Engineering Process and Industrial Systems, National School of Engineers of Gabes, University of Gabes, Tunisia
nidhalmohamedkamel@gmail.com

Lotfi Khezami

Department of Chemistry, College of Science, Imam Muhammad Ibn Saud Islamic University, Saudi Arabia
lkhezami@gmail.com

Mohamed Bououdina

Department of Mathematics and Science, Faculty of Humanities and Sciences, Prince Sultan University, Saudi Arabia
moboudina@gmail.com

Abdelmottaleb Ouederni

Research Laboratory of Engineering Process and Industrial Systems, National School of Engineers of Gabes, University of Gabes, Tunisia
mottaleb.ouederni@univgb.tn

ABSTRACT

In this study, ZnO nanoparticles were successfully synthesized through a sol-gel route using zinc acetate precursor, polymer N-Vinylpyrrolidone (PVP), Cetyl Trimethyl Ammonium Bromide (CTAB), and Poly-Ethylene Glycol (PEG). The nanoparticles were examined with Crystal Violet (CV) dye photodegradation under UV irradiation. The addition of polymers controlled size, shape, and morphology of the particles and reduced the formation of agglomerates. The size and crystallinity of polymer/ZnO nanoparticles were analyzed using X-Ray Diffraction (XRD). UV-visible spectroscopy was used to study the optical properties and bandgap of the nanoparticles, while nitrogen adsorption-desorption isotherms were used to analyze their pore structure and surface area. XRD showed that all the lattice constants changed and the bandgap energy declined with the addition of polymers, which can be attributed to the improvement in crystallinity of the polymer specimens. The ZnO bandgap can be tuned in the range of 3.29, 3.251, 3.275, and 3.254 eV, using pure ZnO, CTAB, PEG, and PVP, respectively. All obtained BET isotherms can be classified as type II isotherms, characteristic of nanoporous material. ZnO-pure has high photocatalytic efficiency (69.66%), which was significantly decreased after the surface of the ZnO nanoparticles was capped with PVP (43.16%), PEG (19.82%), and CTAB (14.36%). On the same surface, the catalytic activity of ZnO-PVP was improved by 28% compared to pure ZnO, with a photodegradation efficiency of 97%.

Keywords-photocatalytic degradation; organic pollutant; sol-gel method; ZnO semiconductor; polymeric-surface modification; mass transfer

I. INTRODUCTION

Organic Dyes (ODs) are currently deemed the primary wastewater contaminants derived from numerous industrial activities: tanning paints, ink, textile, paper, and plastic manufacturing. Approximately 15-20% of ODs are lost during synthesis or processing and discharged into industrial wastewater [1-2]. ODs such as methyl blue, rhodamine B, methyl orange, Congo red, and Crystal Violet (CV) commonly exist in wastewater with concentrations of 5 to 1500 mg/L. These ODs cause severe problems to the environment and the health of living organisms, i.e., they posses carcinogenic and mutagenic consequences, due to their high toxicity [3]. CV is a triarylmethane dye that is used primarily in additives, cosmetics, textile/dyeing, foodstuffs, leather tanning, ballpoint pen, paper, and, more generally, in analytical chemistry factories [4]. Different recent wastewater dye removal methods have been adopted, such as biological processes and chemical oxidation. Alternatively, the treatment of aqueous contaminants using heterogeneous photocatalysis appears to be a process to efficiently remediate wastewater pollution [5-6]. Photocatalysis degenerates the organic contaminants in aqueous solutions through the photogeneration of electron-hole (e^-/h^+) pairs reaction with dissolved oxygen water and hydroxyl ions to form highly reactive radical species such as hydroxyl radicals. These active species can totally or partially transform organic molecules into CO_2 and H_2O.

Avant-garde oxidation procedures are used to remove toxic elements from the environment, employing techniques administered by metal semiconducting nanomaterials of Fe_2O_3, TiO_2, ZnO, CdS, and ZnS that are good photocatalysts [7-8]. Such materials with nanoscale grain size, defined as nanomaterials (NMs), exhibit desirable and unique properties analogous to their bulk counterparts [9-11]. Zinc oxide (ZnO) is an II-VI group of semiconductors that possesses magnetic properties with a potentially broad range of applications due to its exciting binding energy (60 meV at 25°C), relatively high energy bandgap (3.37 eV), and sizeable optical gain. In addition to its structural stability, photosensitivity, and reliable oxidizing capability, ZnO is a non-toxic, abundant, and affordable material [12]. Several physicochemical techniques have been adapted to the synthesis of ZnO NMs either in powder or thin-film structures, i.e., sol-gel route, spray pyrolysis, microwave irradiation, chemical vapor deposition, pulsed laser deposition, and hydrothermal and aqueous solution precipitation [13-14]. The sol-gel process is the most common method used to prepare nanoparticle (NP) materials because of its cost-effectiveness and easiness. During this process, many preparation parameters may influence the properties of the final products, i.e., the nature of the precursors, solvents, catalyst quality, pH, and the temperature and duration of annealing [15-16]. Alternatively, the use of polymer or surfactant agents during the synthesis process directly influences the shape and size, the degree of agglomeration (monodispersed NPs), the surface functionality, and the optical and electrical properties of NPs [17-18]. Furthermore, the synthesis of ZnO nanocrystalline through sol-gel approaches commonly requires surfactants to reduce the long reaction time and improve the poor ZnO crystallinity produced at low temperatures [19-20].

Extensive studies of ZnO nanostructures were devoted to controlling its properties by adding various organic additives, such as polymers or surfactants, during the fabrication process. In [21-22], cetyltrimethylammonium bromide (CTAB) was used to grow Zinc-HDS monocrystal sheets by the wet chemical method. In [23], an easy and efficient approach was proposed to prepare hybrid ZnO/QDs, nanorods, and nanoflowers using the rotation coating procedure that utilizes Sodium Dodecyl Sulfate (SDS). In [24], various techniques such as thermal evaporation, electrodeposition, sputtering, electrospinning, and hydrothermal methods were used to grow well-defined morphologies in nanomaterials, including quantum dots, nanowires, nanorods, nanocages, nanotetrapods, nanoflowers, and nanoforests. The production of these nanostructures is a complex process, and the properties of the final product are greatly influenced by different process parameters. Each synthesis method used specific parameters, resulting in diverse shapes and sizes of the nanostructures. In [25], ZnO crystals were synthesized by the hydrothermal method controlled by various molar ratios of SDS and CTAB. In [26], the influence of the surfactant Polyvinyl Alcohol (PVA) on the optical and morphological characteristics of ZnO nanorods, elaborated through a wet chemical route, was examined. In [27], the evolution of the optical bandgap of ZnO NPs, produced using a sol-gel approach, was investigated due to the surface modification by the poly-4-vinylpyrrolidone (PVP) molecules capping agent. This caping agent maintains the homogeneity of the thin film with significant adhesion to the substrate, mechanical strength, optical quality, and reliable stability. This study investigated the influence of the polymer nature (e.g., PVP, PEG, and CTAB), introduced during the sol-gel procedure, on the phase stability and crystallinity quality, particle morphology and size, agglomeration and surface functionality, the optical and magnetic properties, and photocatalytic activity of uncapped and capped ZnO NPs.

II. EXPERIMENTAL PROCEDURE

A. Preparation of ZnO NPs

ZnO NPs were synthesized using the sol-gel route by mixing zinc acetate (99% purity), surfactants (CTAB, PEG, and PVP), and NaOH (98.5% purity). A distilled water/ethanol (99.9% purity) solvent (2:1 by volume) was used in the experiment. A 0.05 g polymer solution (PVP, PEG, and CTAB) was added, and the respective concentration of $Zn(CH_3COO)_2$ and NaOH solutions was approximately 0.55 $mol.L^{-1}$. 80 mL of $Zn(CH_3COO)_2$ and 160 mL of NaOH solutions were mixed and constantly stirred (600 rpm) at 50°C for 3 hours. A white precipitate was recovered when the mixture was brought to room temperature. The products obtained were centrifuged at 3000 rpm for 5 minutes, filtrated, and abundantly rinsed with acetone solution (99.5% purity) and then distilled water to eliminate residues. The final products were oven-dried under vacuum at 30°C for 12 hours. Similarly, pure ZnO NPs were prepared under identical conditions.

B. Characterizations of ZnO NPs

The structure and crystallinity of the prepared nanopowders were examined by XRD at room temperature using a D8 Advance Bruker diffractometer supplied by Cu-Kα radiation

(λ=0.15406 nm) at an accelerating voltage of approximately 40 kV in the range of 20-80 °C. Particle morphology was analyzed under Transmission Electron Microscopy (TEM) through JEOL, JEM-2100. Pores size, volume, and Specific Brunauer–Emmett–Teller (SBET) surface area were evaluated using nitrogen adsorption-desorption isotherms at 77 K using an ASAP 2020 Micromeritics apparatus. Before each analysis, the samples were outgassed under a vacuum at 100°C for 2 hours. The SBET was evaluated according to the BET equations. The Lippens-de Boer t-plot method estimated the mesopore surface area and micropore volume. The BJH method was used to determine the pore size distribution. The optical properties were evaluated using Diffuse Reflectance Spectroscopy (DRS) using a JASCO V-770 spectrophotometer in the 300-800 nm wavelength interval.

III. RESULTS AND DISCUSSION

A. XRD Analysis

Figure 1 shows the XRD patterns of the prepared ZnO. Irrespective of the nature of the additive polymer, well-illustrated and extended diffraction peaks are observed, where the relative intensity varies slightly. These results indicate the formation of the nanocrystalline phase with good crystallinity. The peaks detected at 2θ of 31.766°, 34.412°, 36.245°, 47.475°, 56.601°, 62.583°, 66.368°, 67.958°, and 69.103° were indexed as reflections (100), (002), (101), (102), (110), (103), (200), (112), and (201) respectively of the hexagonal wurtzite-type structure of the ZnO phase, following JCPDS card No. 36-1451. It can be mentioned that the intensity of (101) reflection is much higher, implying a preferred orientation along the c-axis; ZnO particles grow preferentially along this direction.
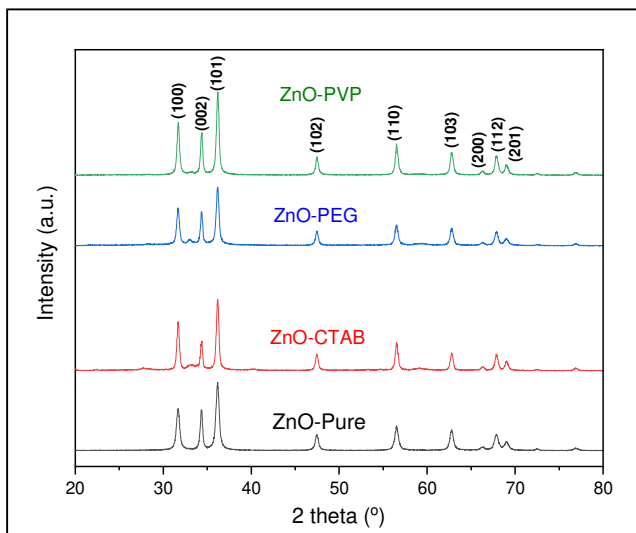
Fig. 1.   XRD patterns of ZnO-Pure, ZnO-CTAB, ZnO-PEG, and ZnO-PVP.

The value of the mean crystallite size (D) was calculated utilizing the Scherer's equation [28-29]:

$$D = \frac{K.\lambda}{\beta.cos\theta} \qquad (1)$$

where K is the shape constant, λ is the wavelength (λ = 0.154056 nm), β is the full width at a half-maximum (FWHM) (i.e., broadening of the peak), and θ is the corresponding diffraction angle. Table I shows the values of crystalline size.

TABLE I.   CRYSTALLITE SIZE AND LATTICE PARAMETERS OF ZNO .

	D (nm)	a (Å)	c (Å)	Band gap (eV)
ZnO-Pure	18	3.256	5.212	3.29
ZnO-CTAB	20	3.2571	5.2146	3.251
ZnO-PEG	21	3.2574	5.2155	3.275
ZnO-PVP	25	3.2578	5.2167	3.254

Table I shows a slight variation that can be associated with the nature of the polymer additive; the value is within the range of 18-25 nm. Nevertheless, the observed slight increase in the crystallite size value may be associated with the polymer's Molecular Weight (MW); the higher the MW, the larger the crystallite size. In addition, it is essential to note that the diameter of semiconductor NPs directly affects the optical and luminescence properties. It is also crucial to note that CTAB, PEG, and PVP polymers play a double role in the reaction medium, stabilizing particles against agglomeration and inhibiting their growth. CTAB, PEG, and PVP will be adsorbed on the surface of the ZnO NP, limiting the diffusion of other species onto the surface of the formed nuclei once they reach the critical diameter. Consequently, the growth rate of ZnO NPs will be inhibited. Meanwhile, the polymeric chain will favor the dispersion of NPs in the solution pending the preparation operation, limiting the agglomeration during centrifugation and annealing in the oven. The lattice constants ($a = b$ and c) of the ZnO wurtzite structure were calculated using the interplanar distance d and h, k, l values of the XRD profile using the following equation [30]:

$$\frac{1}{d^2} = \frac{3}{4}\left[\frac{h^2+h.k+l^2}{a^2}\right] + \frac{l^2}{c^2} \qquad (2)$$

The computed lattice parameters, shown in Table I, are close to the values conveyed in the literature and corroborate those of bulk ZnO according to JCPDS card No. 36-1451. Meanwhile, the lattice parameters are relatively sensitive to the nature of the added polymer. In fact, oth lattice parameters appear to increase compared to pure ZnO $a = b = 3.256$ Å and $c = 5.212$ Å.

B. TEM Observations

Figure 2 shows the TEM images of ZnO NPs. These images were used to investigate the crystalline characteristics and size of the synthesized ZnO polymeric NPs, indicating that the ZnO NPs are slightly agglomerated and confirm the hexagonal structure. The average particle size of all samples ranged from 18 to 30 nm, close to those calculated from the XRD data.

C. BET Analysis

Figures 3 and 4 show the shape of the N_2 adsorption-desorption isotherms and the pore size distribution of ZnO-Pure, ZnO-CTAB, ZnO-PEG, and ZnO-PVP, using knowledge of the pore size, commonly classified as micropore, mesopore or macropore. As shown in Figure 3, the prepared ZnO NP samples reveal a type II adsorption-desorption isotherm with an

H4-type hysteresis loop according to the IUPAC classification. Such a type of hysteresis signifies that the NPs are composed of narrow and irregular slit-like pore shapes with wide diameter distribution and walls formed of ordered mesoporous. At high relative pressure (P/Po), H4-type hysteresis resulted from filling the mesopores by capillary condensation, exhibiting a form of pores that were moderately flatter than cylindrical. Table II shows all the parameters estimated by the BET analysis.
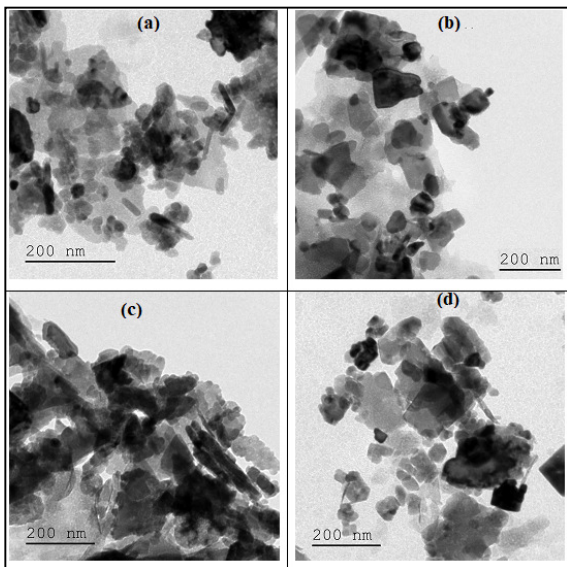
Fig. 2.   TEM images of (a) ZnO-Pure, (b) ZnO-CTAB, (c) ZnO-PEG, and (d) ZnO-PVP.
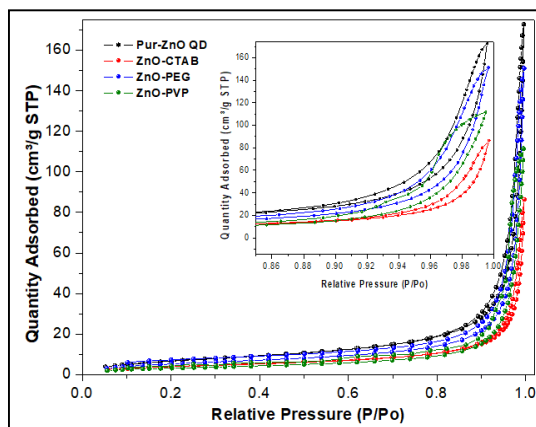
Fig. 3.   Adsorption-desorption isotherms of N$_2$ at 77 K. Gauss model fit in the inset figure.

The SBET gradually decreases, with obviously a decrease in the surface area due to the treatment. As a result of the treatment, the average volume of pores decreases (from 26.44×10^{-2} to 11.92×10^{-2} cm^3.g^{-1}). Inversely, the variation in the average pore diameter is not apparent. The pore size distribution defined by the BJH model from the desorption part of the isotherm (Figure 4 inset) indicates that a significant portion of the pores have diameters ranging from 2 to 200 nm.

Moreover, two zenith peaks center around 125 nm for all nanocomposites except ZnO-PVP, which appears at 70 nm. The ZnO-PVP pore size distribution is in the 2-100 nm interval, having an average pore diameter of about 45 nm. Meanwhile, pure ZnO and ZnO-PEG nanopowder have an average pore diameter of approximately 35.52 and 43.58 nm and broaden in the 2-250 nm range. Concerning the ZnO-CTAB sample, the pore size distribution is broader, as illustrated by the Gaussian fit curves. As can be seen, incorporating the three polymers in the structure of ZnO, even at low content, yields an increase in the SBET and the average pore volume (Table II) and constricts the pore size distribution.
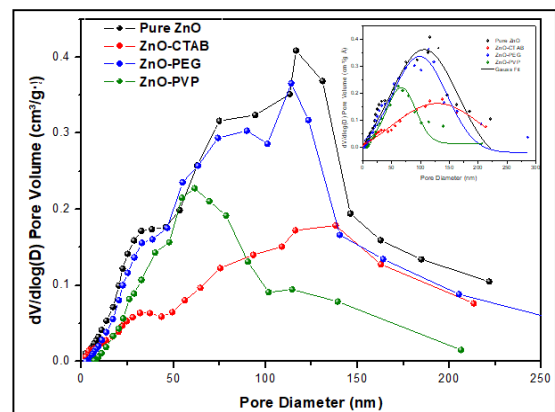
Fig. 4.   Pore size distribution of ZnO-Pure, ZnO-CTAB, ZnO-PEG, ZnO-PVP. Gauss model fit in the inset figure.

TABLE II.   MAIN BET CHARACTERISTICS OF ZNO POWDERS.

	Grain Size (nm)	Average Pore volume (cm^3.g^{-1}) x 10^2	Surface BET (m^2.g^{-1})
ZnO-Pure	18	26.44	26.75
ZnO-CTAB	20	12.55	15.22
ZnO-PEG	21	23.56	20.35
ZnO-PVP	25	12.80	11.92

D. Optical Properties

The bandgap energy value measurements were performed by a UV-visible infrared spectrometer. Figure 5 shows the measured absorption characteristics of pure ZnO and those prepared with PVP, PEG, and CTAB. The lack of jump difference in absorbance intensity due to the effect of PVP, PEG, and CTAB on the particles may be evidence of the ZnO elaboration NPs. Figure 5 also shows that the bandgap absorption in ZnO between 351 and 372 nm displays a tiny shift towards blue accompanying the addition of a small amount of polymers. The blue shift in the ZnO nanostructures may result from the size effect. The bandgap energy of various ZnO samples might be affected by UV-visible spectroscopy absorbance spectra as shown in Figure 6. Since ZnO are direct bandgap semiconductors, their optical absorption edge and bandgap energy meet the following equation [31-32]:

$$(\alpha h \vartheta)^{1/n} = A \left(h \vartheta - E_g \right) \qquad (3)$$

where v is the frequency, a is the absorption coefficient, h is Planck's constant, E_g is the energy bandgap of the semiconductor, A is a proportionality constant, and n is assigned to the electron type for directly allowed transitions. In this study, $n = 1/2$. In the classic route, after the $(ah\theta)^{1/2}$ is sketched versus $(h\theta-E_g)$, the intersection with the x-axis at the tangent of the linear section of the plot yields the bandgap energy value.
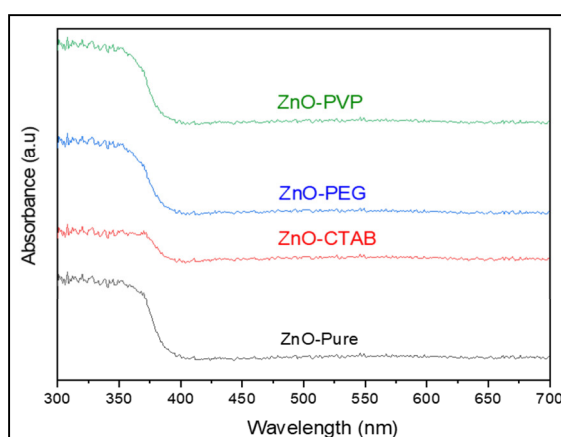
Fig. 5.   UV-visible absorbance spectra of ZnO-Pure, ZnO-CTAB, ZnO-PEG, and ZnO-PVP.
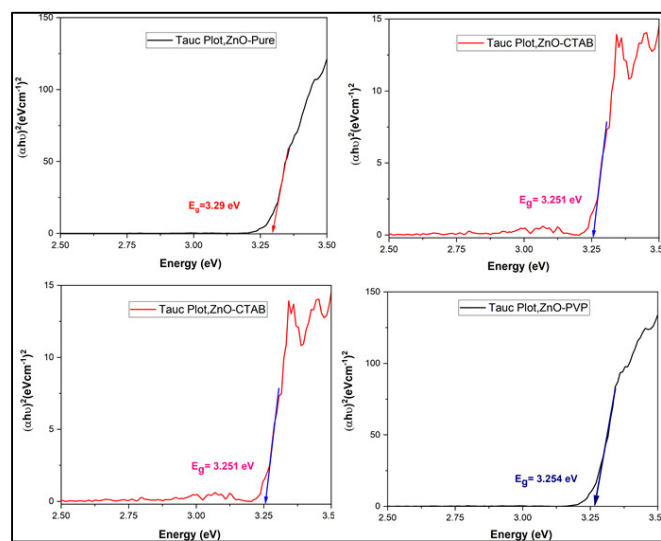
Fig. 6.   Tauc plots of ZnO-Pure, ZnO-CTAB, ZnO-PEG, and ZnO-PVP.

Consequently, as shown in Table I, the bandgap energy values of the samples are very close, which may be attributed to the low number of polymers introduced in the elaboration of NPs. In [32], investigating the elaboration of silver decorated Cu/ZnO photocomposites using the sol-gel route showed that the value of pure ZnO at 3.13 eV and the bulk value of ZnO at 3.37 eV. The narrowing in bandgap energy was attributed to the quantum confinement effect and its association with the reduction of particle size to the nanoscale. The reduction in the optical energy bandgap with polymers might increase the crystalline size, expanding the density of the localized state in

the conduction band. Therefore, it can be deduced that the use of polymers could tune the optical bandgap during the synthesis process.

E. Photocatalytic Activity

CV was used as a model molecule to assess the photocatalytic efficiency of bare and surfactant-capped ZnO NPs in reaction under UV light irradiation. The optical absorption peak of the dye tested at a wavelength of 587 nm was selected to scrutinize the photodegradation operation. Photodegradation was performed using UV lamps operating at 365 nm. The adsorption effect on the surface of ZnO NPs was evaluated under dark conditions for 30 min. 50 ml of 10 mg.L^{-1} CV solution was mixed with 0.1 g of the ZnO or surfactant-capped ZnO NPs in a 100 mL sealed Erlenmeyer flask. The suspension was magnetically agitated (550 rpm) for 180 min at room temperature under UV-light irradiation. Then, the photocatalyst was separated from the CV solution using a centrifuge (6000 rpm) for 4 min. The obtained solution was filtered to eliminate any NPs. The CV concentration at any time of the degradation process was evaluated using a Thermo Scientific Evolution 300 UV-visible spectrophotometer. The photodegradation efficiency (*DE%*) of NPs after 180 min of contact time was estimated using the following equation:

$$DE\% = \left(\frac{C_0 - C_t}{C_0}\right) \times 100 \qquad (4)$$

where C_0 and C_t are the initial and CV concentration at any time t up to 180 min, respectively. Figure 7 shows the degradation efficiency of ZnO NPs for CV photodegradation over time up to 180 min.
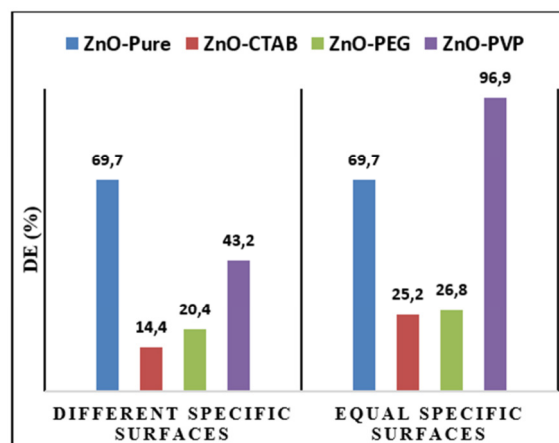
Fig. 7.   Degradation efficiencies of ZnO-Pure, ZnO-CTAB, ZnO-PEG, and ZnO-PVP of CV for different and equal specific surfaces.

ZnO-Pure has a high photocatalytic efficiency (69.66%), which was significantly reduced after the surface of ZnO NPs was coated with PVP (43.16%), PEG (19.82%), and CTAB (14.36%). This result may be explained by the hydrophilicity of bare ZnO NPs because they can attract more CV molecules from water at their surface and be in close contact with air. Surfactant-capped ZnO NPs are hydrophobic, leading to lower photocatalytic efficiency. The surfactants coating the surface of the ZnO NPs interfere with the CV molecules' adsorption and

contact with air. The photodegradation experiments also suggested that a thin film of polymers was developed on ZnO NPs' surfaces, reducing their photocatalytic property. The decrease in photocatalytic efficiency is more significant with lower surfactant molecular weight, i.e., CTAB, PEG, and PVP-capped ZnO NPs, respectively. This phenomenon occurs because as the molecular weight of the capping agent increases, the spatial prevention will upsurge, leading to a reduction in the amount of adsorbed polymer.

From the experimental results, it can be concluded that the phenomena of mass transfer, hydrophilia, and molecular weight are competitive and limiting processes of photocatalytic degradation. On the other hand, to better visualize the effect of the addition of polymers to ZnO NPs, it is interesting to analyze the catalytic activity at the same specific surface. Figure 7 shows that ZnO-PVP is the least influenced by these limitations and that the catalytic activity is very satisfactory with an improvement of 28% compared to pure ZnO, i.e., a photodegradation efficiency of about 97%.

IV. CONCLUSION

In this study, pure, CTAB, PVP, and PEG ZnO NPs were successfully fabricated through an uncomplicated sol-gel process. This innovative approach focuses on the use of polymers as dispersing agents, thus contributing to the dispersion of ZnO NPs inside the polymer matrix. Better interfacial interactions between the NPs and the polymer due to this greater dispersion improve the mechanical characteristics and overall performance of the composite. According to the experimental results, the size, crystallinity, morphology, bandgap, and BET surface of ZnO NPs shifted with the nature of the polymers. The photocatalytic activity of pure and modified ZnO NPs was considered by investigating the CV dye degradation under UV radiation. The photocatalytic degradation process involves several competitive steps, limiting the process and/or delaying the degradation. Hydrophilic behavior, molecular weight, particle size, and specific surface influence photocatalytic degradation. ZnO-PVP presented the best CV conversion rate and appeared to be the least influenced by these limitations.

REFERENCES

[1] H. B. Slama *et al.*, "Diversity of Synthetic Dyes from Textile Industries, Discharge Impacts and Treatment Methods," *Applied Sciences*, vol. 11, no. 14, Jan. 2021, Art. no. 6255, https://doi.org/10.3390/app11146255.

[2] A. Tkaczyk, K. Mitrowska, and A. Posyniak, "Synthetic organic dyes as contaminants of the aquatic environment and their implications for ecosystems: A review," *Science of The Total Environment*, vol. 717, May 2020, Art. no. 137222, https://doi.org/10.1016/j.scitotenv.2020.137222.

[3] P. Suresh, A. M. Umabala, and A. V. P. Rao, "Rapid sun light degradation of Rhodamine-B, Methylene blue, Methyl orange, Congo red and their binary mixtures using suprastoichiometric Bi - Molybdate," *International Journal of Engineering and Applied Sciences*, vol. 2, no. 8, Aug. 2015, Art. no. 257851.

[4] S. Mani and R. N. Bharagava, "Exposure to Crystal Violet, Its Toxic, Genotoxic and Carcinogenic Effects on Environment and Its Degradation and Detoxification for Environmental Safety," in *Reviews of Environmental Contamination and Toxicology Volume 237*, W. P. de Voogt, Ed. Springer International Publishing, 2016, pp. 71–104.

[5] M. M. Nadareishvili, G. Mamniashvili, D. Jishiashvili, G. Abramishvili, C. Ramana, and J. Ramsden, "Investigation of the Visible Light-Sensitive ZnO Photocatalytic Thin Films," *Engineering, Technology & Applied Science Research*, vol. 10, no. 2, pp. 5524–5527, Apr. 2020, https://doi.org/10.48084/etasr.3392.

[6] H. A. Maddah, "Numerical Analysis for the Oxidation of Phenol with TiO2 in Wastewater Photocatalytic Reactors," *Engineering, Technology & Applied Science Research*, vol. 8, no. 5, pp. 3463–3469, Oct. 2018, https://doi.org/10.48084/etasr.2304.

[7] Z. Hafizi and N. Nasr, "The Effect of Zinc Oxide Nanoparticles on Safflower Plant Growth and Physiology," *Engineering, Technology & Applied Science Research*, vol. 8, no. 1, pp. 2508–2513, Feb. 2018, https://doi.org/10.48084/etasr.1571.

[8] R. Ameta, M. S. Solanki, S. Benjamin, and S. C. Ameta, "Chapter 6 - Photocatalysis," in *Advanced Oxidation Processes for Waste Water Treatment*, S. C. Ameta and R. Ameta, Eds. Cambridge, MA, USA: Academic Press, 2018, pp. 135–175.

[9] Y. Yang *et al.*, "BiOX (X = Cl, Br, I) photocatalytic nanomaterials: Applications for fuels and environmental management," *Advances in Colloid and Interface Science*, vol. 254, pp. 76–93, Apr. 2018, https://doi.org/10.1016/j.cis.2018.03.004.

[10] J. Carlos Colmenares and R. Luque, "Heterogeneous photocatalytic nanomaterials: prospects and challenges in selective transformations of biomass-derived compounds," *Chemical Society Reviews*, vol. 43, no. 3, pp. 765–778, 2014, https://doi.org/10.1039/C3CS60262A.

[11] T. Peng and J. A. Lalman, "TiO2 Nanomaterials for Enhanced Photocatalysis," in *Catalysis by Metal Complexes and Nanomaterials: Fundamentals and Applications*, vol. 1317, Washington, DC, USA: American Chemical Society, 2019, pp. 135–165.

[12] P. Uikey and D. K. Vishwakarma, "Review of Zinc Oxide (ZnO) Nanoparticles Applications and Properties," *International Journal of Emerging Technology in Computer Science & Electronics*, vol. 21, no. 2, pp. 239–232, Apr. 2016.

[13] G. Madhumitha, G. Elango, and S. M. Roopan, "Biotechnological aspects of ZnO nanoparticles: overview on synthesis and its applications," *Applied Microbiology and Biotechnology*, vol. 100, no. 2, pp. 571–581, Jan. 2016, https://doi.org/10.1007/s00253-015-7108-x.

[14] M. C. Uribe-López *et al.*, "Photocatalytic activity of ZnO nanoparticles and the role of the synthesis method on their physical and chemical properties," *Journal of Photochemistry and Photobiology A: Chemistry*, vol. 404, Jan. 2021, Art. no. 112866, https://doi.org/10.1016/j.jphotochem.2020.112866.

[15] S. Arya *et al.*, "Review-Influence of Processing Parameters to Control Morphology and Optical Properties of Sol-Gel Synthesized ZnO Nanoparticles," *ECS Journal of Solid State Science and Technology*, vol. 10, no. 2, Oct. 2021, Art. no. 023002, https://doi.org/10.1149/2162-8777/abe095.

[16] M. Parashar, V. K. Shukla, and R. Singh, "Metal oxides nanoparticles via sol–gel method: a review on synthesis, characterization and applications," *Journal of Materials Science: Materials in Electronics*, vol. 31, no. 5, pp. 3729–3749, Mar. 2020, https://doi.org/10.1007/s10854-020-02994-8.

[17] F. Ahangaran and A. H. Navarchian, "Recent advances in chemical surface modification of metal oxide nanoparticles with silane coupling agents: A review," *Advances in Colloid and Interface Science*, vol. 286, Dec. 2020, Art. no. 102298, https://doi.org/10.1016/j.cis.2020.102298.

[18] O. Tavakkoli, H. Kamyab, M. Shariati, A. Mustafa Mohamed, and R. Junin, "Effect of nanoparticles on the performance of polymer/surfactant flooding for enhanced oil recovery: A review," *Fuel*, vol. 312, Mar. 2022, Art. no. 122867, https://doi.org/10.1016/j.fuel.2021.122867.

[19] H. Yu, J. Wang, X. Yan, J. Wang, P. Cheng, and C. Xia, "Effect of surfactants on the morphology and photocatocatalytic properties of ZnO nanostructures," *Optik*, vol. 185, pp. 990–996, May 2019, https://doi.org/10.1016/j.ijleo.2019.04.040.

[20] K. Huszla *et al.*, "UV-light photocatalytic degradation of non-ionic surfactants using ZnO nanoparticles," *International Journal of Environmental Science and Technology*, vol. 19, no. 1, pp. 173–188, Jan. 2022, https://doi.org/10.1007/s13762-021-03160-1.

[21] H. Tang, J. C. Chang, Y. Shan, and S. T. Lee, "Surfactant-Assisted Alignment of ZnO Nanocrystals to Superstructures," *The Journal of*

Physical Chemistry B, vol. 112, no. 13, pp. 4016–4021, Apr. 2008, https://doi.org/10.1021/jp0775707.

[22] S. B. Eadi, S. Kim, and S. W. Jeong, "Effect of Surfactant on Growth of ZnO Nanodumbbells and Their Characterization," *Journal of Chemistry*, vol. 2017, Jul. 2017, Art. no. e1728345, https://doi.org/10.1155/2017/1728345.

[23] S. A. Patil *et al.*, "2D Zinc Oxide – Synthesis, Methodologies, Reaction Mechanism, and Applications," *Small*, vol. 19, no. 14, 2023, Art. no. 2206063, https://doi.org/10.1002/smll.202206063.

[24] S. Kumar, K. Awasthi, and Y. K. Mishra, "4 - Synthesis of ZnO nanostructures," in *Nanostructured Zinc Oxide*, K. Awasthi, Ed. Elsevier, 2021, pp. 93–116.

[25] D. T. Donia *et al.*, "Room Temperature Syntheses of ZnO and Their Structures," *Symmetry*, vol. 13, no. 4, Apr. 2021, Art. no. 733, https://doi.org/10.3390/sym13040733.

[26] A. Kiruthiga, T. Krishnakumar, and R. Kannan, "The effect of surfactant on structural and optical properties of ZnO nanorods by wet chemical synthesis," *AIP Conference Proceedings*, vol. 2142, no. 1, Aug. 2019, Art. no. 150017, https://doi.org/10.1063/1.5122566.

[27] R. B. Asamoah *et al.*, "Synthesis and characterization of zinc and copper oxide nanoparticles and their antibacteria activity," *Results in Materials*, vol. 7, Sep. 2020, Art. no. 100099, https://doi.org/10.1016/j.rinma.2020.100099.

[28] H. S. Wasly, M. S. A. El-Sadek, and M. Henini, "Influence of reaction time and synthesis temperature on the physical properties of ZnO nanoparticles synthesized by the hydrothermal method," *Applied Physics A*, vol. 124, no. 1, Jan. 2018, Art. no. 76, https://doi.org/10.1007/s00339-017-1482-4.

[29] H. Usui, "The effect of surfactants on the morphology and optical properties of precipitated wurtzite ZnO," *Materials Letters*, vol. 63, no. 17, pp. 1489–1492, Jul. 2009, https://doi.org/10.1016/j.matlet.2009.03.054.

[30] C. M. Mahajan, "Structural, Surface Wettability, Optical, Urbach Tail, and Electrical Properties of Spray Pyrolyzed ZnO Thin Films: Role of Air Flow Rate," *JOM*, vol. 75, no. 2, pp. 448–458, Feb. 2023, https://doi.org/10.1007/s11837-022-05621-5.

[31] Z. Chen *et al.*, "Precise control of water content on the growth kinetics of ZnO quantum dots," *Journal of Crystal Growth*, vol. 511, pp. 65–72, Apr. 2019, https://doi.org/10.1016/j.jcrysgro.2019.01.039.

[32] A. Modwi, K. K. Taha, L. Khezami, M. Bououdina, and A. Houas, "Silver decorated Cu/ZnO photocomposite: efficient green degradation of malachite," *Journal of Materials Science: Materials in Electronics*, vol. 30, no. 4, pp. 3629–3638, Feb. 2019, https://doi.org/10.1007/s10854-018-00642-w.